Chapter 8
Three-Dimensional Numerical Analysis of Natural Vibrations and Stability of Cylindrical Shells Interacting with Fluid

Sergey A. Bochkarev, Sergey V. Lekomtsev, Valerii P. Matveenko, and Alexander N. Senin

Abstract Natural vibrations and stability of cylindrical shells interacting with a quiescent and flowing ideal fluid are numerically investigated. A solution is implemented in a three-dimensional formulation using an algorithm that is based on the finite element method. In the numerical examples, shells with an elliptical cross section, coaxial shells, and shells with an eccentricity are considered. The influence of a fluid level inside these structures and axial misalignment on natural frequencies and vibration modes, and the critical velocities of instability are analyzed. Calculations has revealed the peculiarities of the dynamic characteristics of the shells under consideration in case of their partial filling with a fluid. It is shown that the stability of the system can be improved by selecting appropriate geometric parameters.

8.1 Introduction

Thin-walled cylindrical shells are the key structural elements, which are able to withstand considerable loads, strong vibrations or seismic effects. When they interact with fluids, resonance phenomena or loss of stability like flutter and divergence are possible. Dynamic processes that occur in this case can lead to large-amplitude vibrations, instantaneous or fatigue failure of the structure. In the context of the onset of an emergency, the greatest hazards are associated with storage tanks for technological and chemically aggressive fluids located in zones with increased seismic activity; pillars of river bridges; flexible tubes used in the oil-refining and aerospace industries; and different types of heat exchangers employed in power plants (assembly of parallel plates or group of circular cylindrical shells).

Sergey A. Bochkarev · Sergey V. Lekomtsev · Valerii P. Matveenko · Alexander N. Senin
Institute of Continuous Media Mechanics, Ural Branch of Russian Academy of Sciences, 1, Acad. Korolev str., 614068 Perm, Russian Federation,
e-mail: bochkarev@icmm.ru, lekomtsev@icmm.ru, mvp@icmm.ru, senin.a@icmm.ru

H. Altenbach et al. (eds.), *Progress in Continuum Mechanics*,
Advanced Structured Materials 196,
https://doi.org/10.1007/978-3-031-43736-6_8

Distinguishing features in the interaction of shell structures with a quiescent or flowing fluid, as well as with a gaseous medium, have long been studied. An extensive bibliography of papers on this topic is presented in both parts of the well-known monograph [1, 2]. Literature reviews that expand this list of research sources and provide the reader with some pioneering works not mentioned yet can be found in recent articles by the authors [3–8]. Over the past few decades, analysis of the natural vibrations and hydroelastic stability of shells of revolution (cylindrical and conical, coaxial) has been carried out, as a rule, using a variety of numerical-analytical and numerical approaches implemented in an axisymmetric formulation or reduced to it. That is the reason why many significant factors remain unexplored, whose influence on the dynamic characteristics of the system can only be assessed when solving a 3D problem. The circumferential symmetry breaking of a cylindrical shell due to its partial filling with a fluid [9, 10], use of an open [11] or non-circular cross section [12–16], coaxial shells misalignment [7, 8, 17, 18], or due to the impact of spatial force factors, determines the specific behavior of natural vibration frequencies (mode shapes) and stability parameters, which is different from that of similar symmetrical configurations. Bearing in mind that the fluid flow has a destabilizing effect on the elastic shell and leads to significant changes in its dynamic behavior, the above-mentioned factors require careful analysis.

The main research tool used to solve the problems of hydroelasticity, including those of real practical interest, is a finite element method. In contrast to other numerous approaches, it is the most accurate and versatile method because it allows one to overcome the restrictions on the geometry of the structure and on the kinematic boundary conditions at its edges. The available commercial finite element analysis software helps researchers to solve transient, harmonic and modal problems via simulating the interaction of an arbitrary elastic structure and an acoustic environment [19]. However, there is no such possibility for stability problems in the case of a flowing fluid.

In this paper, the findings of studies on the hydroelastic interaction of shell structures asymmetric in the circumferential direction are generalized. The solution is found within the framework of a universal approach that is based on the developed three-dimensional mathematical formulation and its implementation by the finite element method.

8.2 Mathematical and Numerical Formulations

This section briefly describes the mathematical formulation and the corresponding finite element algorithm, which are designed to analyze natural vibrations and stability of three-dimensional thin-walled cylindrical shells in the general case with a non-circular cross section and interacting with an internal steady flow of an ideal compressible fluid. All basic relation are given for the configuration shown in Fig. 8.1, but they can be easily generalized to the case of coaxial [5, 6] and eccentric [8] cylindrical shells.

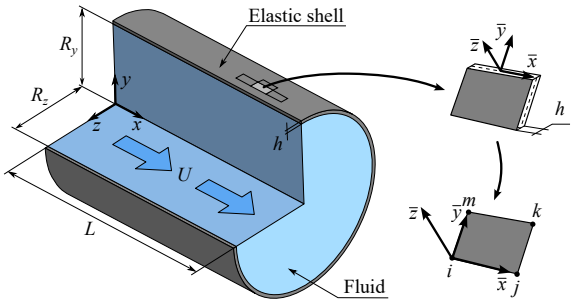

Fig. 8.1: Computational scheme of the elliptical cylindrical shell.

In the case of small perturbations the vortex-free dynamics of an ideal compressible fluid is described by wave equation [2, 20, 21], which is formulated in terms of the perturbation velocity potential ϕ in the global Cartesian coordinate system (x, y, z) and transformed to the weak form together with the impermeability and boundary conditions [21]. Finally, we get:

$$\int\limits_{V_f} \nabla F_m \cdot \nabla \hat{\phi} \mathrm{d}V + \int\limits_{V_f} F_m \frac{1}{c^2} \frac{\partial^2 \hat{\phi}}{\partial t^2} \mathrm{d}V + \int\limits_{V_f} F_m \frac{2U}{c^2} \frac{\partial^2 \hat{\phi}}{\partial t \partial x} \mathrm{d}V -$$
$$- \int\limits_{V_f} F_m \frac{U^2}{c^2} \frac{\partial^2 \hat{\phi}}{\partial x^2} \mathrm{d}V - \int\limits_{S_\sigma} F_m \frac{\partial \hat{\bar{w}}}{\partial t} \mathrm{d}S - \int\limits_{S_\sigma} F_m U \frac{\partial \hat{\bar{w}}}{\partial x} \mathrm{d}S = 0, \quad m = \overline{1, m_f}. \tag{8.1}$$

Here: $\hat{\phi}$ and $\hat{\bar{w}}$ are the trial solutions for the velocity potential ϕ and normal displacements of the thin-walled structure $\bar{w}$; V_f is the volume of fluid; S_σ is the fluid-structure interface; c is the speed of sound in a fluid; t is time; F_m and m_f are the basis functions and their number; U is the velocity of fluid in the direction of the x-axis.

The hydrodynamic pressure acting on the elastic structure wall is calculated using linearized Bernoulli's formula:

$$p = -\rho_f \left(\frac{\partial \phi}{\partial t} + U \frac{\partial \phi}{\partial x} \right), \tag{8.2}$$

where ρ_f is the density of a fluid. We use the following boundary conditions to solve Eq. (8.1):

$$x = 0 : \phi = 0, \quad x = L : \partial \phi / \partial x = 0, \tag{8.3}$$

where L is the length of the structure.

Modeling the shells partially filled with a fluid is based on the assumption that the free surface of the liquid S_{free} does not move and is not under the action of dynamic pressure and surface tension. An appropriate boundary condition is given by [10]:

$$\boldsymbol{x} \in S_{\text{free}} : \phi = 0. \tag{8.4}$$

A curvilinear surface of the structure is represented with sufficient accuracy as a set of flat rectangular segments (Fig. 8.1) [22]. Small strains in each of these segments are determined in the framework of the classical plate theory [23]:

$$\left\{\varepsilon_{\bar{x}\bar{x}}, \varepsilon_{\bar{y}\bar{y}}, \gamma_{\bar{x}\bar{y}}\right\}^{\mathrm{T}} = \left\{\varepsilon^0_{\bar{x}\bar{x}}, \varepsilon^0_{\bar{y}\bar{y}}, \gamma^0_{\bar{x}\bar{y}}\right\}^{\mathrm{T}} + \bar{z}\left\{\varepsilon^1_{\bar{x}\bar{x}}, \varepsilon^1_{\bar{y}\bar{y}}, \gamma^1_{\bar{x}\bar{y}}\right\}^{\mathrm{T}}, \tag{8.5}$$

$$\bar{\boldsymbol{\varepsilon}}^0 = \left\{\varepsilon^0_{\bar{x}\bar{x}}, \varepsilon^0_{\bar{y}\bar{y}}, \gamma^0_{\bar{x}\bar{y}}\right\}^{\mathrm{T}} = \left\{\frac{\partial \bar{u}}{\partial \bar{x}}, \frac{\partial \bar{v}}{\partial \bar{y}}, \frac{\partial \bar{u}}{\partial \bar{y}} + \frac{\partial \bar{v}}{\partial \bar{x}}\right\}^{\mathrm{T}},$$

$$\bar{\boldsymbol{\varepsilon}}^1 = \left\{\varepsilon^1_{\bar{x}\bar{x}}, \varepsilon^1_{\bar{y}\bar{y}}, \gamma^1_{\bar{x}\bar{y}}\right\}^{\mathrm{T}} = \left\{-\frac{\partial^2 \bar{w}}{\partial \bar{x}^2}, -\frac{\partial^2 \bar{w}}{\partial \bar{y}^2}, -2\frac{\partial^2 \bar{w}}{\partial \bar{x}\bar{y}}\right\}^{\mathrm{T}},$$

where $\bar{u}, \bar{v}, \bar{w}$ are the displacements of the points on the middle surface of the plane segment in the direction of the corresponding axes of the Cartesian coordinate system $(\bar{x}, \bar{y}, \bar{z})$ (Fig. 8.1).

The generalized vector $\bar{\boldsymbol{\varepsilon}}$, which contains the middle surface strains $\bar{\boldsymbol{\varepsilon}}^0$ and the curvatures $\bar{\boldsymbol{\varepsilon}}^1$, is written as:

$$\bar{\boldsymbol{\varepsilon}} = \begin{Bmatrix} \bar{\boldsymbol{\varepsilon}}^0 \\ \bar{\boldsymbol{\varepsilon}}^1 \end{Bmatrix} = \left\{\varepsilon^0_{\bar{x}\bar{x}}, \varepsilon^0_{\bar{y}\bar{y}}, \gamma^0_{\bar{x}\bar{y}}, \varepsilon^1_{\bar{x}\bar{x}}, \varepsilon^1_{\bar{y}\bar{y}}, \gamma^1_{\bar{x}\bar{y}}\right\}^{\mathrm{T}}. \tag{8.6}$$

The physical relations between the vector of forces and moments $\bar{\boldsymbol{t}}$ and the vector of generalized strains $\bar{\boldsymbol{\varepsilon}}$ are formulated in the following form:

$$\bar{\boldsymbol{t}} = \left\{N_{\bar{x}\bar{x}}, N_{\bar{y}\bar{y}}, N_{\bar{x}\bar{y}}, M_{\bar{x}\bar{x}}, M_{\bar{y}\bar{y}}, M_{\bar{x}\bar{y}}\right\}^{\mathrm{T}} = \boldsymbol{S}\bar{\boldsymbol{\varepsilon}}, \tag{8.7}$$

where the coefficients entering the matrix $\boldsymbol{S}$ are calculated for isotropic material using Young's modulus E and Poisson's ratio ν by known way [23].

A mathematical formulation of the dynamics problem of thin-walled structure relies on the variational principle of virtual displacements, which takes into account the equation for hydrodynamic pressure (8.2) and the work done by inertial forces. In the absence of external loads it can be written in the matrix form as:

$$\int\limits_{S_s} \delta\bar{\boldsymbol{\varepsilon}}^{\mathrm{T}} \boldsymbol{S}\bar{\boldsymbol{\varepsilon}}\,\mathrm{d}S + \int\limits_{S_s} \delta\bar{\boldsymbol{d}}^{\mathrm{T}} \boldsymbol{J}\ddot{\bar{\boldsymbol{d}}}\,\mathrm{d}S + \int\limits_{S_\sigma} \delta\bar{w}\,\rho_f\left(\frac{\partial\hat{\phi}}{\partial t} + U\frac{\partial\hat{\phi}}{\partial\bar{x}}\right)\mathrm{d}S = 0, \tag{8.8}$$

where $\bar{\boldsymbol{d}} = \{\bar{u}, \bar{v}, \bar{w}, \theta_{\bar{x}}, \theta_{\bar{y}}, \theta_{\bar{z}}\}^{\mathrm{T}}$ is the generalized vector of the thin-walled structure displacements, including rotation angles $\theta_{\bar{x}}, \theta_{\bar{y}}, \theta_{\bar{z}}$ with respect to the corresponding axes of the coordinate system $(\bar{x}, \bar{y}, \bar{z})$; S_s is the shell surface; $\boldsymbol{J} = \mathrm{diag}\,(J_0, J_0, J_0, J_2, J_2, J_2)$ is the inertia matrix, $J_0 = \rho_s h$, $J_2 = \rho_s h^3/12$ and ρ_s is the density of the elastic structure material.

The formulation of the natural vibrations problem is based on the representation

$$\boldsymbol{u}(\boldsymbol{x}, t) = \{\boldsymbol{d}(\boldsymbol{x}, t), \phi(\boldsymbol{x}, t)\}^{\mathrm{T}} = \tilde{\boldsymbol{u}}(\boldsymbol{x})\mathrm{e}^{\mathrm{i}\lambda t}, \tag{8.9}$$

where $\tilde{\boldsymbol{u}} = \left\{\tilde{\boldsymbol{d}}(\boldsymbol{x}), \tilde{\phi}(\boldsymbol{x})\right\}^{\mathrm{T}}$ is the vector function depending only on coordinates $\boldsymbol{x}$; i is the imaginary unit; $\lambda = \omega + \mathrm{i}\gamma$ is the characteristic index; ω is the natural frequency of vibrations; γ is the value, characterizing the damping of the system.

After substituting expression (8.9) into Eqs. (8.1) and (8.8), dividing by the exponent and implementing the known procedures of the finite element method, we obtain a coupled system of equations:

$$\left(-\lambda^2 \boldsymbol{M} + \mathrm{i}\lambda \boldsymbol{C} + \boldsymbol{K} + \boldsymbol{A}\right)\tilde{\boldsymbol{u}} = 0, \tag{8.10}$$

$$\boldsymbol{M} = \begin{bmatrix} \boldsymbol{M}_s & 0 \\ 0 & \boldsymbol{M}_f \end{bmatrix}, \quad \boldsymbol{C} = \begin{bmatrix} 0 & \boldsymbol{C}_{sf} \\ \boldsymbol{C}_{fs} & \boldsymbol{C}_f \end{bmatrix}, \quad \boldsymbol{K} = \begin{bmatrix} \boldsymbol{K}_s & 0 \\ 0 & \boldsymbol{K}_f \end{bmatrix}, \quad \boldsymbol{A} = \begin{bmatrix} 0 & \boldsymbol{A}_{sf} \\ \boldsymbol{A}_{fs} & \boldsymbol{A}_f \end{bmatrix},$$

where typical finite element matrices are determined in a well-known manner [6, 22]:

$$\boldsymbol{M}_f^e = \int\limits_{V_f} \frac{1}{c^2}\boldsymbol{F}^{\mathrm{T}}\boldsymbol{F}\mathrm{d}V, \quad \bar{\boldsymbol{M}}_s^e = \int\limits_{S_s} \boldsymbol{N}^{\mathrm{T}}\boldsymbol{J}\boldsymbol{N}\mathrm{d}S,$$

$$\boldsymbol{C}_f^e = \int\limits_{V_f} \frac{2U}{c^2}\frac{\partial \boldsymbol{F}^{\mathrm{T}}}{\partial x}\boldsymbol{F}\mathrm{d}V, \quad \bar{\boldsymbol{C}}_{fs}^e = -\int\limits_{S_\sigma} \boldsymbol{F}^{\mathrm{T}}\boldsymbol{N}_w\mathrm{d}S, \quad \bar{\boldsymbol{C}}_{sf}^e = \int\limits_{S_\sigma} \rho_f \boldsymbol{N}_w^{\mathrm{T}}\boldsymbol{F}\mathrm{d}S,$$

$$\boldsymbol{K}_f^e = \int\limits_{V_f} (\nabla \boldsymbol{F})^{\mathrm{T}}\nabla \boldsymbol{F}\mathrm{d}V, \quad \bar{\boldsymbol{K}}_s^e = \int\limits_{S_s} \boldsymbol{B}^{\mathrm{T}}\boldsymbol{S}\boldsymbol{B}\mathrm{d}S,$$

$$\boldsymbol{A}_f^e = -\int\limits_{V_f} \frac{U^2}{c^2}\frac{\partial \boldsymbol{F}^{\mathrm{T}}}{\partial x}\frac{\partial \boldsymbol{F}}{\partial x}\mathrm{d}V, \quad \bar{\boldsymbol{A}}_{fs}^e = -\int\limits_{S_\sigma} U\boldsymbol{F}^{\mathrm{T}}\frac{\partial \boldsymbol{N}_w}{\partial x}\mathrm{d}S, \quad \bar{\boldsymbol{A}}_{sf}^e = \int\limits_{S_\sigma} \rho_f U \boldsymbol{N}_w^{\mathrm{T}}\frac{\partial \boldsymbol{F}}{\partial x}\mathrm{d}S.$$

Here: $\boldsymbol{F}, \boldsymbol{N}, \boldsymbol{N}_w$ are the shape functions the trial solutions for the velocity potential of the fluid $\hat{\phi}$, the generalized vector of the nodal displacements of the thin-walled structure $\boldsymbol{d}$ and its normal component $\bar{w}$; $\boldsymbol{B}$ is the gradient matrix, which links the deformation vector with the vector of nodal displacements of the shell finite element. The constitutive relations defined in Eq. (8.5) do not contain the equation for rotation about the axis $\bar{z}$. To eliminate this problem, it is necessary to introduce zero rows and columns and a fictitious moment $M_{\bar{z}}$ into the stiffness matrix [22]. The matrices with overbar ($\bar{\boldsymbol{K}}_s^e$, $\bar{\boldsymbol{M}}_s^e$, $\bar{\boldsymbol{C}}_{sf}^e$, etc.) are formed in the coordinate system $(\bar{x}, \bar{y}, \bar{z})$. Their transformation to the global Cartesian coordinates (x, y, z) is performed for each element using the directional cosine matrix in a known way [6, 22].

In the finite element model, the perturbation velocity potential ϕ, the basis functions F_m, and the membrane displacements of the shell $\bar{u}$ and $\bar{v}$ are described using by Lagrange bi-linear shape functions. The bending displacement $\bar{w}$, the rotation angles $\theta_{\bar{x}}$ and $\theta_{\bar{y}}$ are approximated by the nonconforming cubic Hermite polynomials [22]. The discretization of the computational domains of the fluid and the thin-walled structure is carried out using the spatial 8-node prismatic and flat rectangular finite elements, respectively.

The system of equations (8.10) is converted into the generalized eigenvalue problem [24], which is solved by the implicitly restarted Arnoldi method [25]:

$$\left(\begin{bmatrix} \boldsymbol{C} & \boldsymbol{K}+\boldsymbol{A} \\ -\boldsymbol{I} & 0 \end{bmatrix} + \mathrm{i}\lambda \begin{bmatrix} \boldsymbol{M} & 0 \\ 0 & \boldsymbol{I} \end{bmatrix} \right) \begin{Bmatrix} \mathrm{i}\lambda\tilde{\boldsymbol{u}} \\ \tilde{\boldsymbol{u}} \end{Bmatrix} = 0. \tag{8.11}$$

The model described above and the finite element algorithm allow us to investigate a system of two coaxial or eccentric cylindrical shells with a fluid in the annular gap between them. In this case $\tilde{\boldsymbol{u}} = \left\{\tilde{\boldsymbol{d}}^{(1)}, \tilde{\boldsymbol{d}}^{(2)}, \boldsymbol{\phi}\right\}^{\mathrm{T}}$ and the global matrices in equation (8.10) take the form:

$$\boldsymbol{M} = \begin{bmatrix} \boldsymbol{M}_s^{(1)} & 0 & 0 \\ 0 & \boldsymbol{M}_s^{(2)} & 0 \\ 0 & 0 & \boldsymbol{M}_f \end{bmatrix}, \quad \boldsymbol{K} = \begin{bmatrix} \boldsymbol{K}_s^{(1)} & 0 & 0 \\ 0 & \boldsymbol{K}_s^{(2)} & 0 \\ 0 & 0 & \boldsymbol{K}_f \end{bmatrix}, \tag{8.12}$$

$$\boldsymbol{C} = \begin{bmatrix} 0 & 0 & -\boldsymbol{C}_{sf}^{(1)} \\ 0 & 0 & \boldsymbol{C}_{sf}^{(2)} \\ -\boldsymbol{C}_{fs}^{(1)} & \boldsymbol{C}_{fs}^{(2)} & \boldsymbol{C}_f \end{bmatrix}, \quad \boldsymbol{A} = \begin{bmatrix} 0 & 0 & -\boldsymbol{A}_{sf}^{(1)} \\ 0 & 0 & \boldsymbol{A}_{sf}^{(2)} \\ -\boldsymbol{A}_{fs}^{(1)} & \boldsymbol{A}_{fs}^{(2)} & \boldsymbol{A}_f \end{bmatrix}.$$

where $\tilde{\boldsymbol{d}}^{(1)}$ and $\tilde{\boldsymbol{d}}^{(2)}$ are the generalized vectors of displacements of the inner and outer shells.

The numerical implementation of the finite element algorithm has been carried out in MATLAB software using the capabilities of the ANSYS package to create a mesh. The stability estimation is based on the analysis of complex eigenvalues of problem (8.11), which were obtained under the condition of gradually increasing fluid velocity. In our simulations we consider the shells with different kinematic boundary conditions at the edges and denote them as: F – free edge, S – simple support ($v = w = 0$) and C – rigid clamping ($u = v = w = 0$, $\theta_x = \theta_y = \theta_z = 0$).

8.3 Single Cylindrical Shells

The developed finite-element algorithm was applied to investigate the influence of the fluid level, the ratio of ellipse semi-axes and the linear dimensions on the natural frequencies and mode shapes of vibrations, and the boundary of the hydroelastic stability of circular and elliptical cylindrical shells interacting with quiescent and flowing fluid (Fig. 8.1). The analysis of the obtained results was carried out using the dimensionless quantities, such as the fluid level η, the ellipticity parameter β, the eigenvalue Λ, the natural frequency of vibrations Ω and the flow velocity Y:

$$\eta = \frac{V_f}{V_i}, \ \beta = \frac{R_z}{R_y}, \ \Lambda = \lambda R_y \psi, \ \Omega = \omega R_y \psi, \ \mathrm{Y} = U\psi, \ \psi = \sqrt{\frac{\rho_s\left(1-\nu^2\right)}{E}}, \tag{8.13}$$

where V_i is the volume of the shell interior, R_z and R_y are the ellipse semi-axes (Fig. 8.1). The parameters used in computations are listed in the Table 8.1.

Table 8.1: Computation parameters.

Case	E, GPa	ν	ρ_s, kg/m^3	c, m/s	ρ_f, kg/m^3	R_y, mm	h, mm	L/R_y
I	205	0.3	7800	1500	1000.0	77.25	1.5	2.99
II	206	0.3	7850	1500	1004.8	200	2.0	5.00

8.3.1 Circular Cylindrical Shells

It is known that the empty and fluid-filled vertical circular ($\beta = 1$) cylindrical shells are characterized by the multiple frequencies of the spectrum. They correspond to the symmetric and antisymmetric mode shapes with the same number of circumferential (j) and meridional (m) half-waves, which differ only by rotation in the circumferential direction. When horizontal shells are partially filled, mode shapes with one combination of the wave numbers (m, j) correspond to unequal natural frequencies (Fig. 8.2*a*, *b*). This difference varies and depends on the fluid level η of the structure (Fig. 8.3). The interesting thing about the lowest vibration modes is that, at any values of the parameter η, the displacements are always at a maximum in the fluid-structure interface (Fig. 8.2). A similar conclusion was made earlier in [10].

The change of the six lowest natural vibration frequencies of a horizontal circular cylindrical shells (Case I, $\beta = 1$) in response to the filling level η is shown in Fig. 8.3 for different variants of boundary conditions. It is seen that even a small amount of a fluid inside the structure causes a notable decrease in the vibration frequency, which most significantly affects the shell rigidly clamped at both edges (Fig. 8.3*b*).

Figure 8.4 illustrates the comparison of the natural vibration frequencies of the shells of different orientations depending on the amount of a fluid inside these structures (Case I, $\beta = 1$). In the case of horizontally located shells, we confine ourselves to considering the odd modes Ω_1, Ω_3, Ω_5, since the frequencies of even modes Ω_2, Ω_4, Ω_6 differ only slightly from them (Fig. 8.3). For the vertical configurations, the symmetric and antisymmetric mode shapes have multiple frequencies, and thus

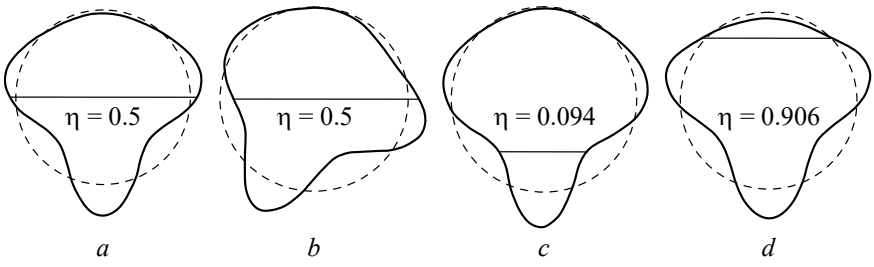

Fig. 8.2: Schematic view of mode shapes of a horizontal cylindrical shell (SS): *a* – $\omega_1 = 282$ Hz, *b* – $\omega_2 = 287$ Hz, *c* – $\omega_2 = 399$ Hz, *d* – $\omega_1 = 265$ Hz.

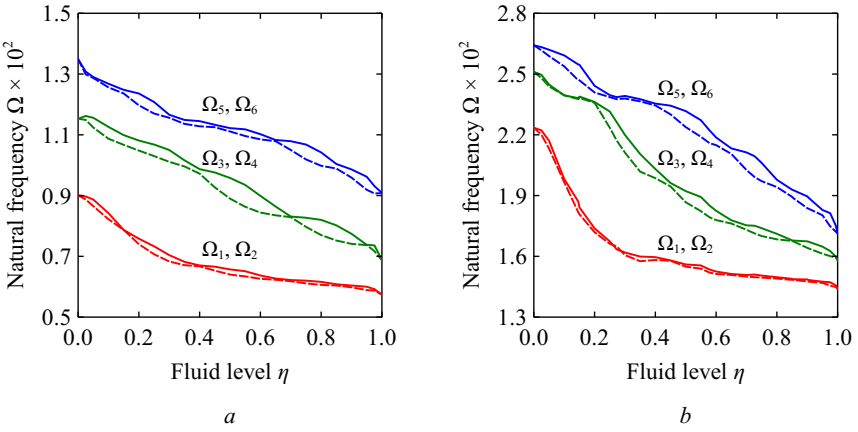

Fig. 8.3: Six lowest natural vibration frequencies of a horizontal cylindrical shell at different fluid level: *a* – CF, *b* – CC.

$\Omega_1 = \Omega_2$, $\Omega_3 = \Omega_4$ and $\Omega_5 = \Omega_6$. Analysis of the obtained dependencies showed that not only the added mass of a fluid but also the hydroelastic interaction on the wetted surface cause significant changes in the spectrum. This is reflected in the fact that, at the same amounts of the fluid, the natural vibration frequencies of the partially filled vertically and horizontally oriented shells fail to coincide in most cases. As seen in Fig. 8.4*a*, the frequencies of the horizontal structure clamped at one edge are lower compared to the vertical one. An exception is almost completely filled shells, for which the difference at $\eta > 0.9$ can be termed insignificant. A more complex dependence is observed under boundary conditions referring to rigid clamping at

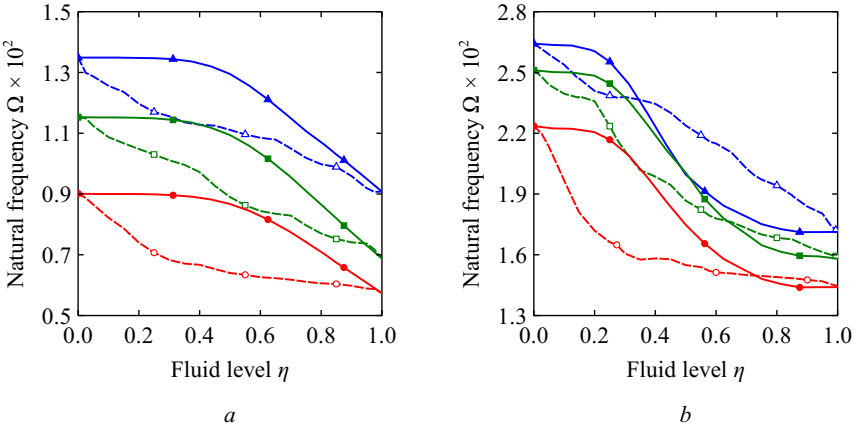

Fig. 8.4: Natural vibration frequencies Ω_1 (○, ●), Ω_3 (□, ■), Ω_5 (△, ▲) of a horizontal (dashed lines) and vertical (solid lines) cylindrical shell at different fluid level: *a* – CF, *b* – CC.

both edges (Fig. 8.4*b*). In this case, situations may arise where the natural vibration frequencies of the systems with different orientations coincide. As an example, we consider the modes Ω_1 and Ω_3 at $\eta \approx 0.72$ and $\eta \approx 0.35$ (the points of intersection of the dashed and solid lines), respectively.

The next example illustrates the problem of hydroelastic stability of a simply supported cylindrical shell (SS) interacting with an internal fluid flow (Case II, $\beta = 1$). The analytical solution of this problem at complete filling ($\eta = 1$) was derived in work [26]. It was found that, under such conditions for fixing the structure, the loss of stability occurs through divergence. With an increase in the flow velocity, the lowest natural frequency of the system decreases until it becomes equal to zero at $\mathrm{Y} = \mathrm{Y}_D$. At this moment, there appears a pair of imaginary parts of this mode, one of which is negative. Considering the results presented in Fig. 8.5, it follows that an increase in the length of the shell L leads to a noticeable decrease in the critical velocity of divergence Y_D. This dependence exhibits a non-monotonic character that can be attributed to the change in the vibration mode, according to which the loss of stability is implemented. As a result, the curve has a break, after which, instead of the local region of increase, the region of decrease appears. Fig. 8.5 shows that a decrease in the fluid level η leads to an increase in the critical velocities of instability. The calculation results demonstrate that the type of stability loss remains the same in this case. Dotted line in Fig. 8.5 corresponds to the results obtained in the framework of the two-dimensional formulation using the semi-analytical finite element method. The presented data illustrate the identity of the found critical velocities for different linear dimensions.

8.3.2 Elliptical Cylindrical Shells

In the numerical examples given in this section, horizontally located elliptical cylindrical shells (Case I) are considered. The study of the results revealed several

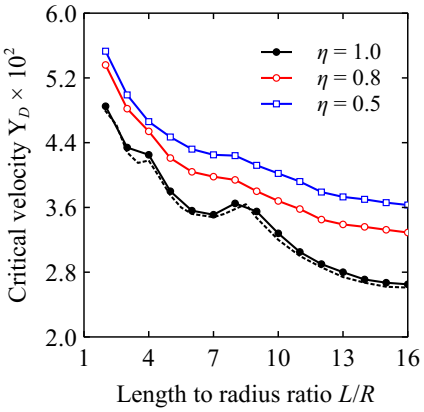

Fig. 8.5: Dimensionless critical velocities of divergence Y_D for circular cylindrical shells as a function of the ratio L/R.

distinguishing features in the behavior of the lowest natural frequencies of vibrations of these structures [3]. Analysis of the effect of the ellipticity parameter β was performed assuming that the size of the vertical semi-axis R_y is kept constant, unless otherwise specified. In this case a change in the value of β is associated with a monotonic change in the cross-sectional area of the shell and the fluid level in it at a fixed value of η.

Figure 8.6*a* shows that the presence of even a small amount of a fluid inside the horizontal circular and elliptical cylindrical shells promotes a significant decrease in their lowest natural frequency of vibrations. Moreover, at $\beta < 1$ it monotonically decreases over the entire range of the values of the parameter η and at $\beta > 1$ becomes an asymptotic dependence. It is seen that when a certain fluid level is reached, the frequency ceases to change from its further increase (Fig. 8.6*a*). The threshold value η, at which the asymptotic behavior occurs, is determined by the ellipticity parameter. This feature is clearly visible in Fig. 8.6*b*, where several curves begin to merge with each other at $\beta > 1.2$.

It should be noted that the dependence of the lowest natural frequency on the ellipticity parameter β exhibits the non-monotonic behavior (Fig. 8.6*b*) and reaches its maximum at $\beta < 1$. This feature is caused by a change in the vibration mode and is illustrated in more detail in Fig. 8.7 for the shells completely filled with a fluid. At $\beta = 1$, the frequencies corresponded to the symmetric and antisymmetric mode shapes with one combination of wave numbers (m, j) coincide. However, at $\beta \neq 1$, there may be more than two modes with the same number of half-waves in the longitudinal and circumferential directions. In this case, only the lowest frequency mode is taken into account. As can be seen from Fig. 8.7*a*, the lowest natural vibration frequency is determined by the frequencies which correspond to three mode shapes with different numbers of circumferential half-waves ($j = 2, 3, 4$). The deviation of the cross section of the shell from the circular profile due to a change in the ellipticity parameter leads

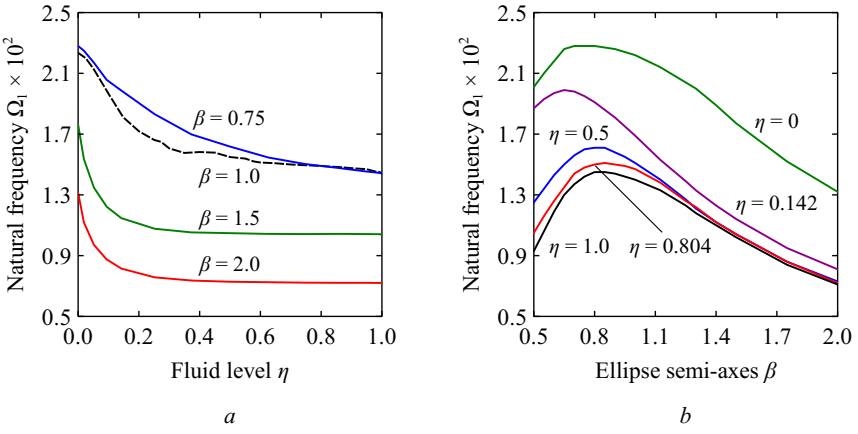

Fig. 8.6: The lowest natural vibration frequencies of an elliptical cylindrical shell (CC) at different fluid level (*a*) and ratio of ellipse semi-axes (*b*).

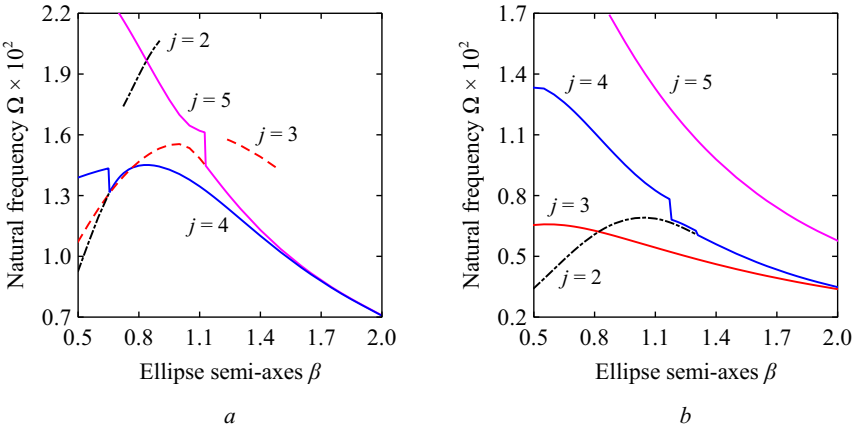

Fig. 8.7: Natural vibration frequencies of an elliptical cylindrical shells completely filled with a fluid ($m = 1$): a – CC, b – CF.

to a non-uniform rigidity of the structure along the circumferential coordinate. In turn, this contributes to the appearance of various vibration mode shapes. The jumps in frequency were driven by the degeneration of one of the vibration modes and its transformation to a new one. For example, at $\beta \approx 1.13$, mode $(1,3)$ converts into $(1,5)$. With a further increase in the parameter β, mode $(1,3)$ is not realized on the considered frequency spectrum, but it appears again, starting from $\beta \approx 1.24$. The features mentioned above continue to exist at another variant of the kinematic boundary conditions. The dependence of the lowest natural vibration frequency of the shell fixed at one edge on the ellipticity parameter is also nonmonotonic and has a pronounced extremum (at $\beta = 0.82$). As one can see in Fig. 8.7*b*, the number of circumferential half-waves changes at this point from $j = 2$ to $j = 3$.

It is also important to point out one more feature previously determined for the horizontal circular cylindrical shells and which is preserved for elliptical one. The maximum height of the half-waves in the circumferential direction of the lowest vibration mode is observed on the fluid-structure interface. For the vibration modes corresponding to the highest frequencies of the spectrum, this pattern does not always manifest itself.

The dependencies of the critical velocities of instability of the completely filled simply supported cylindrical shells with circular and elliptical cross-sections on the ratio L/R_y are shown in Fig. 8.8*a*. In both cases, the divergence boundary significantly depends on the linear dimensions of the structure. With an increase in the length of the shell L, the critical velocities Y_D decrease. The kinks of the curves are due to a change in the mode according to which the loss of stability occurs. For example, for the shell with $\beta = 1.5$ the number of circumferential half-waves j changes from $j = 4$ to $j = 3$ at $L/R_y > 5$.

In the next series of examples, the hydroelastic stability of the partially filled shells clamped at both edges is considered at different ratios of the ellipse semi-axes.

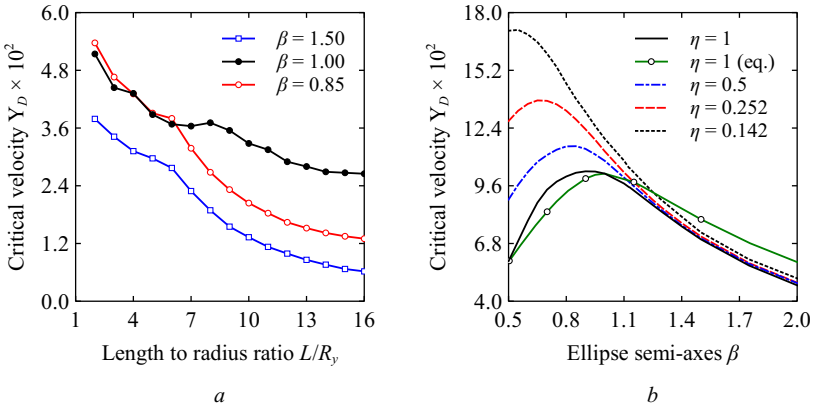

Fig. 8.8: Dimensionless critical velocity of instability Y_D for elliptical cylindrical shells depend on the ratio L/R_y (*a*) ($\eta = 1$, Case II, SS) and the ratio of the ellipse semi-axes (*b*) (Case I, CC).

Analysis of the results presented in Fig. 8.8*b* indicates that a decrease in the fluid level η leads to an increase in the critical flow velocities Y_D. However, there are such values of η and β, starting from which the value of Y_D changes insignificantly (at $\beta > 1.25$, the curves almost coincide). In the case of a quiescent fluid, the dependence of the lowest natural vibration frequency of such structures on the ellipticity parameter β has an extremum, which is observed at $\beta < 1$ and shifts depending on the fluid level (Fig. 8.6*b*). Figure 8.8*b* shows that this feature is also characteristic of the critical flow velocities. In both cases, everything is explained by the fact that the cross-sectional area of the cylindrical shell is not a constant value at a change in β (since $R_y = const$). Further, we will consider the situation where the ellipticity parameter changes and the cross-sectional area of the shell remains equal to a similar circular configuration. The results obtained are shown as line with circles in Fig. 8.8*b*. In this example, there is no difference between the critical velocities at $\beta > 1$ and $\beta < 1$, and the given dependence has a maximum at $\beta = 1$.

8.4 System of two Circular Cylindrical Shells

In this section we consider examples, which are concerned with two horizontally oriented circular cylindrical shells (Fig. 8.9), and use the following parameters:
isotropic shells

$$L^{(1)} = L^{(2)} = L = 1 \text{ m},\ R^{(2)} = 0.1 \text{ m},\ h^{(1)} = h^{(2)} = h = 5 \times 10^{-4} \text{ m},$$
$$E^{(1)} = E^{(2)} = E = 200 \text{ GPa},\ \nu^{(1)} = \nu^{(2)} = \nu = 0.3,\ \rho_s^{(1)} = \rho_s^{(2)} = \rho_s = 7800 \text{ kg/m}^3,$$

ideal fluid

$$\rho_f = 1000 \text{ kg/m}^3,\ c = 1500 \text{ m/s}.$$

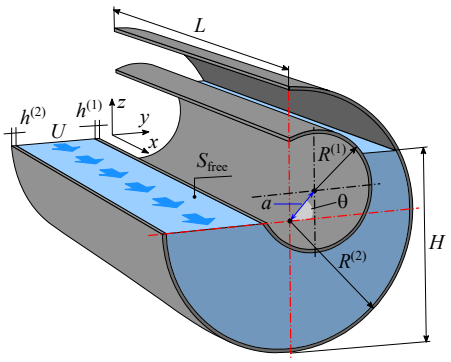

Fig. 8.9 Section of eccentric cylindrical shells with the annular gap partially filled with a flowing fluid.

The computations were done for different values of the dimensionless annular gap between them, which is defined as $k = \left(R^{(2)} - R^{(1)}\right)/R^{(1)}$. In the analysis of the influence of the fluid level H, consideration is given only to such values of H at which both shells remain wetted. This yields to the following condition:

$$\left(R^{(2)} - R^{(1)}\right) \le H \le 2R^{(2)}. \tag{8.14}$$

Hereinafter, superscripts "(1)" and "(2)" denote the inner and outer shells, respectively. The obtained results are represented in terms of dimensionless quantities. Some of them are given in expressions (8.13) and new ones are defined below:

$$\eta = \frac{H}{2R^{(2)}}, \quad \Lambda = \lambda R^{(1)}\psi, \quad \Omega = \omega R^{(1)}\psi, \quad \xi = \frac{a}{\left(R^{(2)} - R^{(1)}\right)}, \tag{8.15}$$

where η is the fluid level, ξ is the eccentricity (Fig. 8.9), a is the distance between the rotation axes of the shell.

8.4.1 Coaxial Shells

As has been shown previously, the violation of circumferential symmetry of the horizontally oriented shells partially filled with a fluid causes the frequency spectrum to split. For this reason, the frequencies for the mode shapes with the same combination of wave numbers are different, which is shown in Fig. 8.10*a* for $k = 1/10$. In the calculations, it was assumed that the inner elastic shell is clamped at both edges (CC), and the outer shell is absolutely rigid. The natural frequencies of vibrations of such configuration, corresponding to symmetric and antisymmetric modes, coincide when the annular gap is completely filled ($\eta = 1$). When the fluid level decreases in this gap ($\eta < 1$), they begin to differ from each other, and their further change goes along different branches. Another limiting case corresponds to the configuration with ($\eta = 0$). Under such conditions, the frequency spectrum will be closest to the

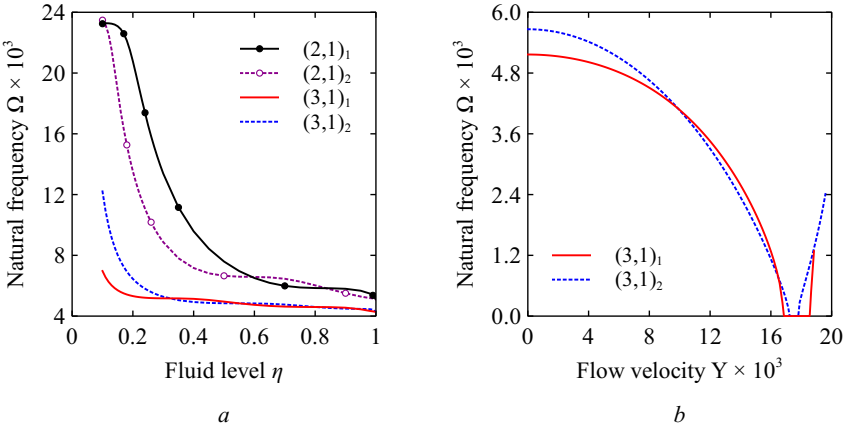

Fig. 8.10: Dependencies of the natural frequencies Ω on the fluid level η (*a*) and the flow velocity Y at $\eta = 0.25$ (*b*) for the outer rigid shell ($k = 1/10$, CC).

vibrations of shells with air in the annular gap, and different branches will coincide. By virtue of Eq. (8.14), this situation cannot arise at all frequencies. On the other hand, the dependencies presented in Fig. 8.10*a* for the same combination of wave numbers (j,m) clearly demonstrate that in some cases the coincidence between symmetric and antisymmetric components also takes place at the values ($\eta > 0$).

Figure 8.10*b* shows the variation of the natural frequencies with the same set of wave numbers (j,m) depend on the flow velocity Y. It follows from the graphs that, when the annular gap is only partially filled with fluid, there is no qualitative difference in the behavior of the presented curves. In particular, the imaginary parts of these two modes do not merge together due to their proximity, and the instability mode remains unchanged.

Figure 8.11 presents the dependencies of the lowest natural frequencies Ω_1 and the critical flow velocities Y_D on the dimensionless fluid level η in the annular channel at different values of k. This example illustrates the case when two elastic coaxial shells are rigidly clamped at their edges. The above graphs show that a decrease in the fluid level leads to an increase in both frequencies and critical velocities. This behavior occurs due to a decrease in the total area of wetted surfaces and is associated with diminishing the role of the added mass of a fluid. The wavy character of the curves in Fig. 8.11*a* is associated with the alternation of the minimum values corresponding to the vibration modes with the same combination of wave numbers. A rapid change in the quantities under study is observed at a low fluid level η for the gap $k = 1/100$. Similar results were obtained for the partial filling of single shells [3, 5]. This phenomenon occurs only at small values of k due to the need for the existence of a wetted surface of the inner shell, that may be absent when the amount of a fluid in a relatively wide annular channel is small (see condition (8.14)). As in the case of complete filling ($\eta = 1$), an increase in the annular gap (Fig. 8.11*b*) and in the rigidity of the outer shell causes the critical velocities to increase as well . Thus,

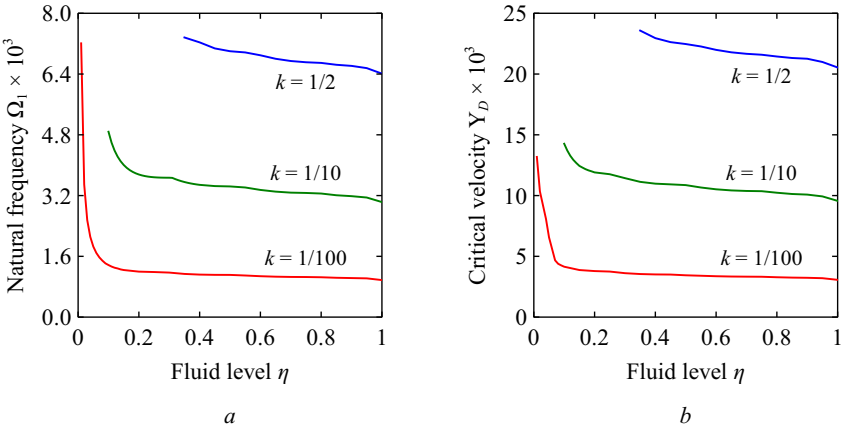

Fig. 8.11: Dependencies of the lowest natural frequencies Ω_1 (*a*) and critical velocities of instability Y_D (*b*) on the fluid level η at different values of the annular gap k.

the narrower is the annular channel (i.e., the smaller is k), the greater is the range within which the fluid level has little effect on the characteristics under consideration.

8.4.2 Eccentric shells

During operation or due to the imperfect shell manufacturing process, the alignment of coaxial shells can be broken. In [8] the influence of the eccentricity ξ and the angle θ, characterizing, respectively, the value and direction of axial deviation of the inner shell is described in detail. It was shown that, when the annular gap is completely filled with fluid and the body forces are absent, the angle θ does not affect the stability boundary, while the eccentricity (ξ increases in absolute value) reduces critical velocity.

In the case of partial filling, the picture becomes much more complicated. When the inner shell is displaced along the free surface, the added mass of the liquid is redistributed. This reduces the critical velocity, regardless of the direction of axial deviation ($\theta = 0°$ or $\theta = 180°$) and the fluid level η. The angle $\theta = 90°$ and the positive values of eccentricity ξ ($\xi > 0$) characterize the rise of the inner shell out of the fluid. In response to the changes in the wetted surface area and to the hydrodynamic pressure redistribution, the critical flow velocities increase or decrease, respectively. The size of the annular gap k has no qualitative effect on the dependence of the critical velocities Y_D on the inner shell eccentricity. A decrease in the value of k leads to a decrease in the stability boundary. This has been established previously for the coaxial cylindrical shells in case of full or partial filling of the annular channel [2, 6].

The results demonstrate that, as the filling level η increases, the influence of the angle θ on the stability boundary decreases until it ceases to have any effect in case of complete filling. The minimum critical velocity Y_D is always obtained at the same eccentricity ($\xi \approx -1$) regardless of the values of θ and η. As for the maximum value of Y_D, it can be achieved at different values of eccentricity on the half-interval $\xi \in [0;\ 1)$ through the selection of θ and η. As noted earlier, this is explained by changes in the inner shell wetted surface and in the fluid added mass. These statements are true when the values of the angle θ are positive, and the negative values of ξ match positive values, though in the direction of the negative angles θ. Furthermore, the data presented in Fig. 8.12 can be arguments for the existence of such configurations in which, subject to proper selection of all parameters, the higher hydroelastic stability threshold than obtained at the coaxial shells can be provided.

The dependencies of the critical velocity Y_D on the angle θ and the eccentricity of the inner shell ξ are presented in Fig. 8.12*b*. When the angle θ decreases, there is such a range of its values where the Y_D remains unchanged. The calculations showed in [8] that, as the fluid level increases, the size of this interval increases as well until the angle θ ceases to affect the stability boundary in the case of full filling (the straight line is parallel to the abscissa axis). At the same time, with an increase in the eccentricity ξ the critical velocity Y_D changes over a wide range (Fig. 8.12*b*), thus providing more opportunities to control dynamic behavior of such structures.

Figures 8.13 and 8.14 gives the mode shapes of the shells for $k = 1/10$ at different variants of annular gap filling, assuming that the value and direction of axial deviation of the inner shell are also different. For each configuration, the flow velocity was set close to the critical value Y_D. In the figures, the dotted lines denote the non-deformed shells, and the solid lines correspond to the deformed one; the fluid level is given in grey. In the spatial mode shapes, the displacements are scaled for clarity in presentation of the data on the relative maximum value of the given configuration.

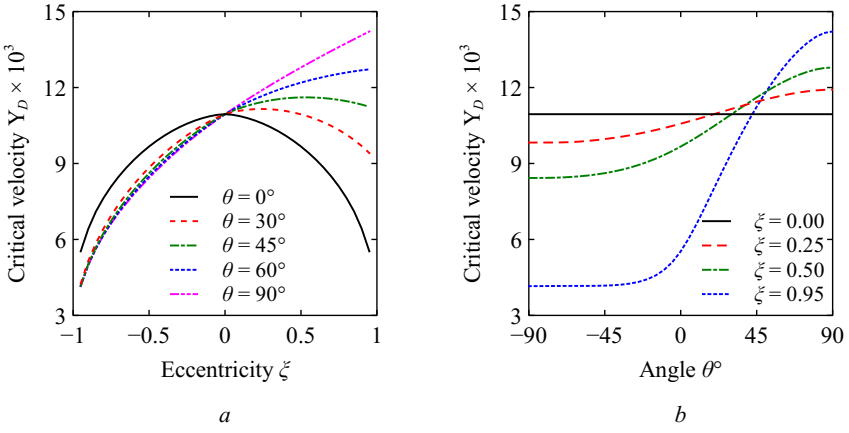

Fig. 8.12: Dependencies of the critical velocities Y_D for $k = 1/10$ at $\eta = 0.5$ on the excentricity ξ at different values of the angle θ (*a*) and the angle θ at different values of excentricity ξ (*b*).

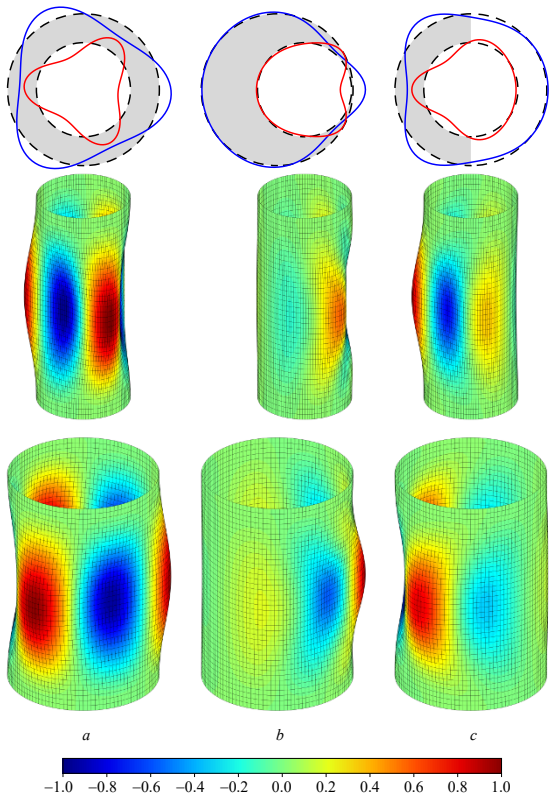

Fig. 8.13: Mode shapes of eccentric shells interacting with the fluid (the cross section at $x = L/2$, the inner and outer shells) for $k = 1/10$ at $\mathrm{Y} \approx \mathrm{Y}_D$: $a - \eta = 1$, $\xi = 0$; $b - \eta = 1$, $\xi = 0.95$, $\theta = 90°$; $c - \eta = 0.5$, $\xi = 0$.

Red and blue on the color scale indicates the displacement in the direction of the outer normal to the shell surface and in the opposite them.

For the completely filled coaxial shells ($\eta = 1, \xi = 0$), the circumferential half-waves have the same height, the size of which is different for the inner and outer shells. In the presence of eccentricity ($\eta \neq 0$), their height within the same shell becomes different. The maximum displacements occur in the surface areas, which correspond to the minimum distance between the shells. With a decrease in the fluid level ($\eta < 1$), there appear half-waves of different heights, while the maximum displacements develop on those parts of the surfaces which interact with the fluid. For the partially filled eccentric structures, the largest half-wave size is observed on the wetted surfaces. Based on the data, we can come to a conclusion that the fluid level of the annular gap has a greater effect on the displacement of the shells subject to vibrations than the eccentricity.

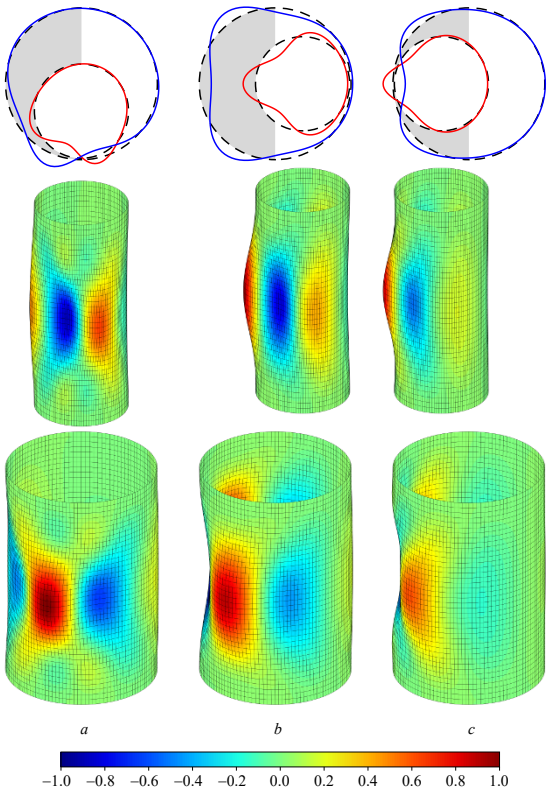

Fig. 8.14: Mode shapes of eccentric shells interacting with the fluid (the cross section at $x = L/2$, the inner and outer shells) for $k = 1/10$ at $\mathrm{Y} \approx \mathrm{Y}_D$: $a - \eta = 0.50$, $\xi = 0.95$, $\theta = 0°$; $b - \eta = 0.50$, $\xi = 0.95$, $\theta = 90°$; $c - \eta = 0.5$, $\xi = 0$, $\theta = -90°$.

8.5 Conclusion

Natural vibrations and stability of cylindrical shells interacting with quiescent and flowing fluid has been investigated in a three-dimensional formulation based on the proposed mathematical model and developed finite element algorithm. In the first group of numerical examples single circular and elliptical cylindrical shells with different boundary conditions, linear dimensions and filling level were analyzed. In another part of the calculations, we studied a system of two coaxial and eccentric circular cylindrical shells. The influence of the fluid level, the annular gap size, the value and direction of axial deviation of the inner shell on the natural vibration frequencies and hydroelastic stability boundary were investigated. The obtained results can be summarized as follows:

- horizontal cylindrical shells partially filled with fluid can have more than two mode shapes with the same number of half-waves in the circumferential and the meridional directions, which correspond to different natural frequencies of vibrations;
- small amount of the fluid in horizontal circular, elliptical and coaxial cylindrical shells lead to an essential decrease in the lowest vibration frequency;

- the lowest natural vibration frequency of horizontal elliptical cylindrical shells has a local extremum, which depends on the fluid level and the ratio of ellipse semi-axes;
- a decrease in the fluid level leads to a growth of the critical flow velocities;
- an increase in the structure length decreases the critical flow velocities;
- for coaxial cylindrical shells with narrow annular gap there is a wide range of the fluid level in which it has little effect on the lowest natural frequency of vibrations and critical velocity of instability;
- hydroelastic stability threshold of the eccentric circular cylindrical shells can be improved by selecting appropriate value and direction of axial deviation of the inner shell.

Acknowledgements The research was carried out in the framework of the government order, state registration number of theme AAAA19-119012290100-8.

References

[1] Païdoussis MP (2014) Fluid-structure Interactions: Slender Structures and Axial Flow, vol 1, 2nd edn. Elsevier Academic Press, London
[2] Païdoussis MP (2016) Fluid-structure Interactions: Slender Structures and Axial Flow, vol 2, 2nd edn. Elsevier Academic Press, London
[3] Bochkarev SA, Lekomtsev SV, Matveenko VP (2016) Natural vibrations and stability of elliptical cylindrical shells containing fluid. Int J Struct Stabil Dyn **16**(10), 1550076
[4] Bochkarev SA, Lekomtsev SV, Matveenko VP (2016) Dynamic analysis of partially filled non-circular cylindrical shells with liquid sloshing. Int J Appl Mech **8**(3), 1650027
[5] Bochkarev SA, Lekomtsev SV, Senin AN (2019) Analysis of the spatial vibrations of coaxial cylindrical shells partially filled with a fluid. J Appl Mech Tech Phy **60**(7):1249–1263
[6] Bochkarev SA, Lekomtsev SV, Matveenko VP, Senin AN (2019) Hydroelastic stability of partially filled coaxial cylindrical shells. Acta Mech **230**(11):3845–3860
[7] Bochkarev SA, Lekomtsev SV, Senin AN (2019) Analysis of spatial vibrations of piezoceramic eccentric cylindrical shells interacting with an annular fluid layer. Fract Struct Integr **13**(49):814–830
[8] Bochkarev SA, Lekomtsev SV, Senin AN (2020) Numerical modeling of eccentric cylindrical shells partially filled with a fluid (in Russ.). J Samara State Tech Univ, Ser Phys Math Sci **24**(1):95–115
[9] Ergin A, Price WG, Randall R, Temarel P (1992) Dynamic characteristics of a submerged, flexible cylinder vibrating in finite water depths. J Ship Res **36**(2):154–167

[10] Amabili M (1996) Free vibration of partially filled, horizontal cylindrical shells. J Sound Vib **191**(5):757–780
[11] Selmane A, Lakis AA (1997) Vibration analysis of anisotropic open cylindrical shells subjected to a flowing fluid. J Fluids Struct **11**(1):111–134
[12] Sewall JL, Pusey CG (1971) Vibration study of clamped-free elliptical cylindrical shells. AIAA J **9**(6):1004–1011
[13] Soldatos KP (1999) Mechanics of cylindrical shells with non-circular cross-section: A survey. Appl Mech Rev **52**(8):237–274
[14] Xiang Y, Huang Y (2005) A novel semi-analytical method for solving acoustic radiation from longitudinally stiffened infinite non-circular cylindrical shells in water. Acta Mech Solida Sin **18**(1):1–12
[15] Kumar A, Patel BP (2018) Nonlinear dynamic response of elliptical cylindrical shell under harmonic excitation. Int J Non-Lin Mech **98**:102–113
[16] Firouz-Abadi RD, Noorian MA, Haddadpour H (2010) A fluid–structure interaction model for stability analysis of shells conveying fluid. J Fluids Struct **26**(5):747–763
[17] Jeong KH (1999) Dynamics of a concentrically or eccentrically submerged circular cylindrical shell in a fluid-filled container. J Sound Vib **224**(4):709–732
[18] Jhung MJ, Jeong KH, Hwang WG (2002) Modal analysis of eccentric shells with fluid-filled annulus. Struct Eng Mech **14**(1):1–20
[19] ANSYS (2022) Release 2022 R1 Documentation. Canonsburg
[20] Il'gamov MA (1969) Vibrations of Elastic Shells Containing Liquid and Gas (in Russ.). Nauka, Moscow
[21] Bochkarev SA, Lekomtsev SV, Matveenko VP (2016) Hydroelastic stability of a rectangular plate interacting with a layer of ideal flowing fluid. Fluid Dynam **51**(6):821–833
[22] Zienkiewicz OC, Taylor RL (2000) The Finite Element Method, vol 1, 5th edn. Butterworth-Heinemann, Oxford
[23] Reddy JN (2015) An Introduction to Nonlinear Finite Element Analysis, 2nd edn. Oxford University Press, London
[24] Tisseur F, Meerbergen K (2001) The quadratic eigenvalue problem. SIAM Rev **43**(2):235–286
[25] Lehoucq RB, Sorensen DC (1996) Deflation techniques for an implicitly restarted Arnoldi iteration. SIAM J Matrix Anal Appl **17**(4):789–821
[26] Weaver DS, Unny TE (1973) On the dynamic stability of fluid-conveying pipes. J Appl Mech **40**(1):48–52